ARTICLE

Traditional Medicine Research 2024;9(11):62. https://doi.org/10.53388/TMR20240229002

Integrated network pharmacology and metabolomics to explore the mechanisms of Shenzao dripping pill against chronic myocardial ischemia

Jie-Hui Kuang[1, 2, 3], Tao Hu[1, 2, 3], Lu-Yong Zhang[1, 4], Yu-Feng Yao[1, 2, 3*], Ming-Hua Xian[1, 2, 3*], Shu-Mei Wang[1, 2, 3, 5*]

[1]School of Chinese Materia Medica, Guangdong Pharmaceutical University, Guangzhou 510006, China. [2]Key Laboratory of Digital Quality Evaluation of Chinese Materia Medica of State Administration of Traditional Chinese Medicine, Guangdong Pharmaceutical University, Guangzhou 510006, China. [3]Engineering & Technology Research Center for Chinese Materia Medica Quality of the Universities of Guangdong Province, Guangdong Pharmaceutical University, Guangzhou 510006, China. [4]Guangzhou Key Laboratory of Construction and Application of New Drug Screening Model Systems, Guangdong Pharmaceutical University, Guangzhou 510006, China. [5]Traditional Chinese Medicine Resource Germplasm Bank Management Center, Yunfu 527500, China.

[*]**Correspondence to:** Yu-Feng Yao, Ming-Hua Xian, Shu-Mei Wang. School of Chinese Materia Medica, Guangdong Pharmaceutical University, No. 280, Waihuan East Road, Higher Education Mega Center, Panyu District, Guangzhou 510006, China. E-mail: yaoyufeng@gdpu.edu.cn; xmh360@163.com; gdpuwsm@126.com.

Abstract

Background: Shenzao dripping pill (SZDP) is empirically prescribed for treating cardiac diseases. Nevertheless, there is a lack of comprehensive knowledge regarding the underlying mechanisms contributing to its therapeutic effects. The objective of this study is to investigate the underlying mechanism of SZDP against chronic myocardial ischemia (CMI) in a rat model. **Methods:** In this study, we utilized electrocardiographic and echocardiographic detection along with pathological tissue analysis to evaluate the efficacy of SZDP. The integration of network pharmacology and metabolomics was conducted to investigate the mechanisms. Molecular docking and molecular dynamics simulations were used to validate the binding energy between the compounds of SZDP and the associated targets. **Results:** The results showed that SZDP was able to improve T wave voltage, reverse CMI abnormalities in ejection fraction and fractional shortening, and restore histopathological heart damage. Metabolomics results indicated that disturbances of metabolic profile in CMI rats were partly corrected after SZDP administration, mainly affecting purine metabolism. 13-Docosenamide may be the potential metabolic biomarker of the therapeutic application of SZDP for CMI. Integrating network pharmacology and metabolomics, thiopurine S-methyltransferase (TPMT), xanthine dehydrogenase/oxidase (XDH), bifunctional purine biosynthesis protein ATIC (ATIC), and cytochrome p450 1A1 (CYP1A1) were identified as possible targets of SZDP to exert therapeutic effects by enhancing the metabolic levels of L-Tryptophan, Deoxyribose 1-phosphate and Phosphoribosyl formamidocarboxamide. **Conclusion:** SZDP has a therapeutic effect on CMI by regulating metabolite levels, acting on the targets of TMPT, XDH, ATIC, and CYP1A1, and reducing cardiomyocyte injury and myocardial fibrosis.

Keywords: chronic myocardial ischemia; metabolomics; network pharmacology; serum metabolites; Shenzao dripping pill

Author contributions

Kuang JH wrote the manuscript and performed the experiments. Hu T performed the experiments and data analysis. Yao YF performed the experiments and helped revise the manuscript. Xian MH designed and supervised this study and helped revise the manuscript. Zhang LY and Wang SM designed and supervised this study. The final manuscript had been approved by all the authors.

Competing interests

The authors declare no conflicts of interest.

Acknowledgments

This research was funded by Scientific and Technological Planning Project of Guangzhou City (Grant No. 201803010115), Projects of The National Natural Science Foundation of China (Grant No. 82173972), 2021 Traditional Chinese Medicine (Medicine of South China) Industry Talents Project-Innovation Team of South China Medicine Resources, Guangdong Provincial Basic and Applied Basic Research Fund (Grant No. 2023A1515011147). It was also supported by the Key Unit of Chinese Medicine Digitalization Quality Evaluation of State Administration of Traditional Chinese Medicine.

Peer review information

Traditional Medicine Research thanks all anonymous reviewers for their contribution to the peer review of this paper.

Abbreviations

SZDP, Shenzao dripping pill; CMI, chronic myocardial ischemia; TCM, traditional Chinese medicine; ECG, electrocardiogram; VIP, variable importance in projection; EF, ejection fraction; FS, fractional shortening; TTC, 2,3,5-Triphenyltetrazolium chloride; AST, aspartate aminotransferase; CK, creatine phosphokinase; LDH, lactate dehydrogenase; HE, hematoxylin and eosin staining; PCA, principal components analysis; OPLS-DA, orthogonal partial least squares discriminant analysis; MD, molecular dynamics; BP, biological process; CC, cell component; MF, molecular function; TPMT, thiopurine S-methyltransferase; XDH, xanthine dehydrogenase/oxidase; ATIC, bifunctional purine biosynthesis protein ATIC; CYP1A1, cytochrome p450 1A1; LVH, left ventricular hypertrophy; RMSD, root mean square deviation; RMSF, root mean square fluctuation; FAICAR, Phosphoribosyl formamidocarboxamide; AICAR, 5-aminoimidazole-4-carboxamide ribonucleotide; AChE, acetylcholinesterase.

Citation

Kuang JH, Hu T, Zhang LY, Yao YF, Xian MH, Wang SM. Integrated network pharmacology and metabolomics to explore the mechanisms of Shenzao dripping pill against chronic myocardial ischemia. *Tradit Med Res.* 2024;9(11):62. doi: 10.53388/TMR20240229002.

Executive editor: Jing-Yi Wang.

Received: 29 February 2024; **Accepted:** 29 April 2024; **Available online:** 07 May 2024.

Traditional Medicine Research 2024;9(11):62. https://doi.org/10.53388/TMR20240229002

Highlights

13-Docosenamide was the potential metabolic biomarker of the therapeutic application of Shenzao dripping pill for chronic myocardial ischemia. Shenzao dripping pill can enhance the metabolic levels of L-Tryptophan, Deoxyribose 1-phosphate and Phosphoribosyl formamidocarboxamide to treat chronic myocardial ischemia. Thiopurine S-methyltransferase (TPMT), xanthine dehydrogenase/oxidase (XDH), bifunctional purine biosynthesis protein ATIC (ATIC), and cytochrome p450 1A1 (CYP1A1) were identified as possible targets of Shenzao dripping pill to exert therapeutic effects on chronic myocardial ischemia.

Medical history of objective

Ischemic heart disease is classified as "Xiongbi" in traditional Chinese medicine theory, and its symptoms resemble heart pain and chest distress. Shenzao dripping pill, a medical prescription derived from traditional Chinese medicine Suhexiang pill that comes from *Su Shen Liang Fang* and was co-authored by Shi Su and Kuo Shen (1075 C.E.), treats the condition known as "Xiongbi" through the modulation of Qi and eliminating blood stasis (enhancing body vital energy, hemodynamic flow, and dissipating blood clots).

Background

One of the leading causes of cardiovascular disease death is ischemic heart disease, a significant public health concern with a high incidence that seriously threatens people's health and closely correlates with cardiac dysfunction [1]. Chronic myocardial ischemia (CMI) is mainly caused by atherosclerosis of the coronary arteries with myocardial hypoxia. CMI is harmful to cardiomyocytes and reduces the function of the heart, which induces myocardial infarction, myocardial fibrosis, and heart failure [2, 3]. CMI is classified as "Xiongbi" in traditional Chinese medicine (TCM) theory, and its symptoms resemble heart pain and chest distress. "Qi" is the strength to empower the whole body. According to TCM, "Qi deficiency" and "blood stasis" are the leading causes of "Xiongbi", and therefore, the treatment approach focuses on regulating Qi to reduce pain and encouraging blood circulation to eradicate blood stasis.

Although the hard work of searching for and developing effective medicines to improve CMI is ongoing worldwide, mortality and morbidity continue to increase [4, 5]. The use of TCM in improving CMI is effective, adequate, and satisfactory. Differing from chemically synthesized medications with adverse drug responses, TCM has the features of multi-ingredient and multi-target [6–8]. TCM can offer many advantages as a therapeutic strategy to prevent or improve CMI [9–11]. Shenzao dripping pill (SZDP) is a clinical-empirical Chinese medicine for heart disease treatment. SZDP comprises six specific herbs, namely *Choerospondiatis Fructus* (Guangzao), *Salviae Miltiorrhizae Radix et Rhizoma* (Danshen), *Ginseng Radix et Rhizoma* (Renshen), *Dalbergiae Odoriferae Lignum* (Jiangxiang), *Styrax* (Suhexiang), and *Borneolum* (Bingpian) [12]. According to TCM theory, SZDP can regulate Qi, relieve pain, and promote blood circulation. In addition, the six herbs that make up SZDP contain medicinal components that have been shown to improve CMI. Recent investigations have shed light on the therapeutic properties of SZDP's constituents, predominantly encompassing organic acids, flavonoids, and saponins, in relation to the cardiovascular system. Some researchers have discovered that total flavonoids in Choerospondias Axillaris can improve arrhythmic and CMI [13, 14]. Protocatechualdehyde, caffeic acid, salvianolic acid C, and other components in *Salviae Miltiorrhizae Radix et Rhizoma* have protective effects of anti-inflammatory and immune regulation on the cardiovascular system. Besides, ferulic acid and salvianolic acid B can work together to enhance angiogenesis and inhibit platelet aggregation [15, 16]. Similarly, *Ginseng Radix et Rhizoma*, *Dalbergiae Odoriferae Lignum*, *Styrax*, and *Cinnamomum camphora* all possess therapeutic components that aid in the treatment of CMI [17–21]. Additionally, we identified the potential therapeutic components of SZDP in our prior study [22, 23]. However, the pharmacological effects and underlying metabolic mechanisms of SZDP are still unknown.

Metabolomics has emerged as a valuable tool for assessing metabolite trends and reflecting in vivo physiological changes. This approach holds promise for predicting, diagnosing, and gaining insights into the mechanisms of treating cardiovascular disease [24–26]. Among the various analytical techniques employed in metabolomics, liquid chromatography-mass spectrometry (LC-MS) stands out due to its exceptional resolution and sensitivity, enabling more precise metabolite identification. Network pharmacology is a widely used approach to exploring the potential mechanism of action of TCM [27–29]. The aim of this investigation was to screen out the active ingredients of SZDP and build a drug-ingredient-target-disease network map utilizing network pharmacology for exploration of the potential molecular mechanisms of SZDP treating CMI. Furthermore, we identify changes in biomarker expression associated with SZDP therapy in CMI rats, explore potential metabolic pathways, and examine the impact of SZDP on CMI-related metabolic disorders from a metabolomics perspective. Finally, the underlying mechanisms of SZDP against CMI were elucidated by combining network pharmacology and Metabolomics. These investigations will offer a crucial theoretical foundation for the clinical application of SZDP.

Methods

Animals and experimental design

The Center of Laboratory Animals' animal ethics committee of Boji Pharmaceutical Co., Ltd. (Guangzhou, China) approved the animal studies that were carried out for this study with the registration number IACUC-N2106-PD. The animal experiments were performed in accordance with the Technical Guidelines for General Pharmacological Research on Chinese Medicines and Natural Medicines in China. Specific pathogen-free male rats (age 6–8 weeks and weight 180–240 g) were procured from Hunan Silaikejingda Laboratory Animal Co., Ltd. (Changsha, China) in the Sprague-Dawley strain with the approval number SCXK-Xiang-2019-0004. The animals were kept in a specific pathogen-free grade laboratory, maintaining a temperature range of 20 to 30 °C and humidity between 55 to 70%. The rats were also given unlimited access to food and water and a 12-h cycle of light and darkness. The CMI rat model was established by ligating the coronary artery. Following an acclimation period, the rats were randomly assigned to various groups for the experiment, including the control group (n = 9), the Sham-operated group (n = 10), the CMI model group (n = 11), the Carvedilol group (n = 10), the low dose of the SZDP administration group (n = 10), the high dose of the SZDP administration group (n = 11).

Materials and reagents

SZDP was provided by Boji Pharmaceutical Co., Ltd. (product batch number 20201228; Guangzhou, China). Carvedilol was procured from Shandong Qilu Pharmaceutical Group Co., Ltd. (batch number 0H0214D26; Jinan, China). CMC-Na was bought from Sinopharm Chemical Reagent Co., Ltd. (product batch number 20191216; Shanghai, China). Zoletil 50 was purchased from Virbac S.A. (product batch number BN7VU4A; Carros, France). Xylazine Hydrochloride Injection was purchased from Jilindunhua ShenDa Animal Pharmaceutical Co., Ltd. (product batch number 20210301; Dunhua, China). Lidocaine Hydrochloride injection was obtained from Guangxi Yuyuan Pharmaceutical Co., Ltd. (product batch number 20201106; Qinzhou, China). HE staining solution was obtained from Wuhan Servicebio Biotechnology Co., Ltd. (product number G1076-500ML; Wuhan, China). Masson's trichrome Staining solution was obtained from Wuhan Servicebio Biotechnology Co., Ltd. (product number G1006-100ML; Wuhan, China). 2,3,5-Triphenyltetrazolium chloride (TTC) was obtained from Sigma-Aldrich (St. Louis, MO, USA).

Aspartate aminotransferase (AST), creatine phosphokinase (CK), and lactate dehydrogenase (LDH) activity assay kits were obtained from Ningbo Meikang Biotechnology Co., Ltd. (product number MS1231, MS2062, MS2252; Ningbo, China).

Drug administration

During the experimental period of 28 days, rats in the control, model, and sham groups were given a solution of 0.5% CMC-Na; in the Carvedilol group was administered 10 mg/kg Carvedilol; in the low dose of the SZDP group was administered 167 mg/kg SZDP; and in the high dose of the SZDP group was administered 500 mg/kg SZDP. After the anterior descending branch was ligated, all rats were subjected to intragastric administration once daily for 28 days.

Electrocardiographic and echocardiographic analysis

After a duration of 4 weeks of treatment, electrocardiograms (ECGs) were conducted. The 1-min surface lead II ECG data was recorded and analyzed by the BL-420F biological signal acquisition and analysis system. All rats underwent transthoracic echocardiography under a mixture of Xylazine Hydrochloride Injection (2 mg/kg) and Zoletil 50 (10 mg/kg) anesthesia to assess the impact of SZDP on the structure and function of the heart by utilizing the ultrasound B-scanner (system MyLab40HD by Esaote, Genova, Italy) with an 18-MHz transducer. Measurements of the thickness of the wall and chamber diameters were used to compute the left ventricle's ejection fraction (EF) and fractional shortening (FS).

Biochemical indicator measurement

Blood was collected and stood for 30 min at room temperature. Then, the blood was subjected to centrifugation at 3,000 rpm and 4 ˚C for 10 min. The serum was collected to detect AST, LDH, and CK activities. Commercial kits were used to measure LDH and CK activities following the instructions.

Histopathological examination

The procedure for hematoxylin and eosin staining (HE) staining was as follows: after the dissection of the heart, samples were washed with saline and promptly preserved with a 10% neutral buffered formalin solution. After the samples were then embedded in paraffin wax, slices (4 μm in thickness) were cut and dewaxed with xylene and ethanol. The slices were stained with hematoxylin stain after being washed with distilled water. Then, the slices were washed with distilled water, and the nucleus was stained with 1% hydrochloric acid. A solution of lithium carbonate was used to enhance the staining of the nucleus. The eosin dye solution was used to stain the slices. The slices were placed in different concentrations of alcohol for dehydration. Finally, all slices were coverslipped with a neutral mounting medium resin. The grading scheme for cardiomyocyte injury was as follows: 0 = not present, 1 = minimal (< 5%), 2 = slight (5–10%), 3 = moderate (11–20%), and 4 = high (> 30%).

The procedure for Masson's trichrome staining was as follows: paraffin slices were dewaxed with xylene and ethanol. Distilled water was used for washing the slices. Lapis lazuli blue dye solution and hematoxylin were used to stain the slices. After rinsing with water, the slices were treated with 1% hydrochloric acid and alcohol, followed by washing. Then, the slices were stained with a ponceau acid fuchsin dye solution and treated with 1% phosphomolybdic acid, bright green, 1% glacial acetic acid, ethanol, and xylenes. Finally, all slices were coverslipped with a neutral mounting medium resin. The percentage of myocardial fibrosis was performed by Image-Pro Plus 6.0.

The procedure of TTC staining was as follows: Hearts were removed and frozen at −80 ˚C for 10 min. Then, the hearts were cut into 1mm sections and incubated with 2% TTC for 30 min at 37 ˚C. Finally, all sections were fixed with 10% formaldehyde.

Network pharmacology analysis

The TCMSP (https://old.tcmsp-e.com/tcmsp.php) database was used to obtain the active components and targets of SZDP with scores of drug-like activity ≥ 0.18 and oral bioavailability ≥ 30%. The SEA (https://sea.bkslab.org/) database was used to screen the targets of the components of SZDP in the blood in our prior study. CMI-related targets were searched from the TTD (https://www.db.idrblab.net/ttd/), GeneCards (https://www.genecards.org/), PharmGkb (https://www.pharmgkb.org/), DisGeNET (https://www.disgenet.org/), OCMIM (https://www.ncbi.nlm.nih.gov/omim), and DrugBank (https://www.drugbank.ca/). The Venn diagram was used to find the common targets from SZDP component-related targets and CMI-related targets.

The common targets were input to the STRING database (https://string-db.org/) to establish the protein-protein interaction (PPI) network. The analysis was limited to "*Homo sapiens*" as the species, and a confidence threshold of 0.4 was applied to guarantee the precision of the outcomes. Then, the PPI network file was imported into Cytoscape (v3.10.0) to screen the core targets using the CytoNCA tool. The "SZDP-herbs-components-targets-CMI" network was constructed using Cytoscape. The GO and KEGG pathway enrichment analyses were performed using common targets.

Serum sample pretreatment for metabolomic analysis

The serum samples were retrieved from the refrigerator at −80 ˚C and placed on crushed ice until the samples were thawed at a low temperature. To precisely precipitate the protein in each 200 μL aliquot of a serum sample, 600 μL of acetonitrile was added, and the mixture was thoroughly mixed for 1 min. Then, the mixture was subjected to centrifugation at 13,000 rpm and 4 ˚C for 15 min. The supernatant was collected and evaporated to dryness with nitrogen. Methanol (100 μL) was added, and the reconstituted mixture was vortexed and centrifuged at 13,000 rpm and a temperature of 4 ˚C for 15 min. The resulting supernatant was collected for further analysis. To assess the repeatability and stability of this experiment, quality control (QC) samples were collected from each test sample and pretreated with the same process as the test samples.

UHPLC-Q-Exactive Orbitrap-MS analysis

The experiment was conducted using a U3000 UHPLC-Q-Exactive Orbitrap MS (Thermo Fisher Scientific Corp., Waltham, MA, USA) equipped with an ACQUITY UPLC BEH C18 column (2.1 mm × 100 mm, 1.7 μm). The solvents A and B comprised the mobile phase, composed of water with 0.1% (volume ratio) formic acid and acetonitrile. The gradient program was as follows: 0–2 min, 5% B; 2–5 min, 5%–50% B; 5–6 min, 50% B; 6–18 min, 50%–100% B. The column was balanced for 4 min before running the sample. The column temperature was kept at 40 ˚C, and the flow rate was fixed at 0.4 mL/min. Each sample run involved injecting 5 μL. Mass spectrometry was set to positive and negative ion switching modes using an electrospray ionization source at 350 ˚C. The specific MS conditions were established: the sheath gas flow rate was 55 arb. Units; the auxiliary gas flow rate was 15 arb. Units with a temperature of 200 ˚C; the electrospray voltage was 3.5 kV in positive ion mode and −3.8 kV in negative ion mode.

Metabonomic data processing and analysis

All original data underwent various processing steps utilizing the Compound Discoverer software 3.0. These pretreatment procedures included peak alignment, peak extraction, and normalization. Key parameters such as retention time, peak intensity, and mass charge ratio were obtained. Subsequently, the processed data were imported into SIMCA-P software (version 14.1) for analysis using principal components analysis (PCA) and orthogonal partial least squares discriminant analysis (OPLS-DA). The validity of the OPLS-DA models was assessed using permutation tests (200 permutations). The significant differential metabolites were obtained using variable importance in projection (VIP) and Student's t-test (*P*-value) with a threshold of VIP > 1 and $P < 0.05$. The differential metabolites were identified by matching with the Human Metabolomes Database (https://www.hmdb.ca) and were imported into MetaboAnalyst (https://www.metaboanalyst.ca/) to analyze metabolic pathways.

Molecular docking analysis and molecular dynamics (MD)

simulations

AutoDock Tools (version 1.5.7) and PyMOL were used for molecular docking and visual analysis. The structure of SZDP compounds was obtained from PubChem and optimized to the minimum energy state by Chem3D. The targets were obtained from the Protein Data Bank database (https://www.rcsb.org/). An adequate docking box wrapped around the active pocket was to cover the protein after removing the organic and solvent. The binding energy was assessed by AutoDock Vina.

MD simulations were performed with GROMACS using the CHARMM36 and AMBER force fields. Ligand topology was obtained from PubChem and Chem3D. Protein topology was generated in the Protein Data Bank database. The ligands and proteins need to be parameterized separately, and the ligands are assigned base coordinates based on the positions documented in the RCSB. The protein-ligand complex was placed in the box after charge-balancing ions containing water molecules. Energy minimization was performed before the simulations began. Production simulations were performed for 100 ns. A time step length of 2 fs was used for all simulations.

Statistical analysis

The statistical analysis was performed on the data, which were expressed as mean ± SD. Compared with the T test, single-factor variance analysis, or two-factor variance analysis, and TuKey inspection were performed by GraphPad Prism 9.0. A *P*-value less than 0.05 was regarded as statistically significant.

Results

Evaluation of the CMI model and treatment effect of SZDP

The electrocardiography results indicated that the T wave in the sham and control groups maintained a horizontal position (Figure 1A). In contrast, the T wave voltage recorded in the model group showed a significant downward shift, close to 0.2 mV, confirming the successful establishment of the CMI model. Following the administration of SZDP, the T wave voltage rose compared to the model group. It approached the same level as in the control group and was close to the levels observed in the Carvedilol group. This suggested that SZDP effectively treated CMI. A quantitative echocardiography analysis was carried out to assess the CMI model and validate the therapeutic impact of SZDP on CMI rats (Figure 1B). The EF and FS indexes were not significantly different in the Sham group compared to the control group. The Sham group's EF and FS indices did not differ substantially from the control group's EF and FS indices. However, the model group's EF and FS index reduction levels were noticeably higher than those of the Sham group, indicating evident cardiomyocyte damage (Figure 1C, 1D). In contrast to the model group, the SZDP-H group therapy significantly improved these indicators, suggesting that it can improve heart function in rats with CMI.

Biochemical indicator measurement results

AST, LDH, and CK were selected for measurement, and no significant differences were found in myocardial function with comparison among multiple groups (Supplementary Figure S1).

SZDP improved histological injury of myocardium in CMI rats

Myocardial fibrosis was obvious in rats after modeling, and the anterior wall of the myocardium was thinned, and the results of TTC staining could not reflect the results of the SZDP efficacy well (Supplementary Figure S2), so the myocardial infarction area calculation was not carried out for this index. The H&E-stained heart sections of the control and sham groups exhibited myocardial cells arranged regularly with normal cell morphology and had well-defined boundaries with ample cytoplasm (Figure 2A). Conversely, the results of the model group showed local serious necrobiosis and intercellular bleeding, accompanied by a large amount of inflammatory cell infiltration. Similar to what was seen in the Carvedilol group, the degree of inflammatory cell infiltration, intercellular hemorrhage, and cardiomyocyte injury all decreased after SZDP treatment (Figure 2C).

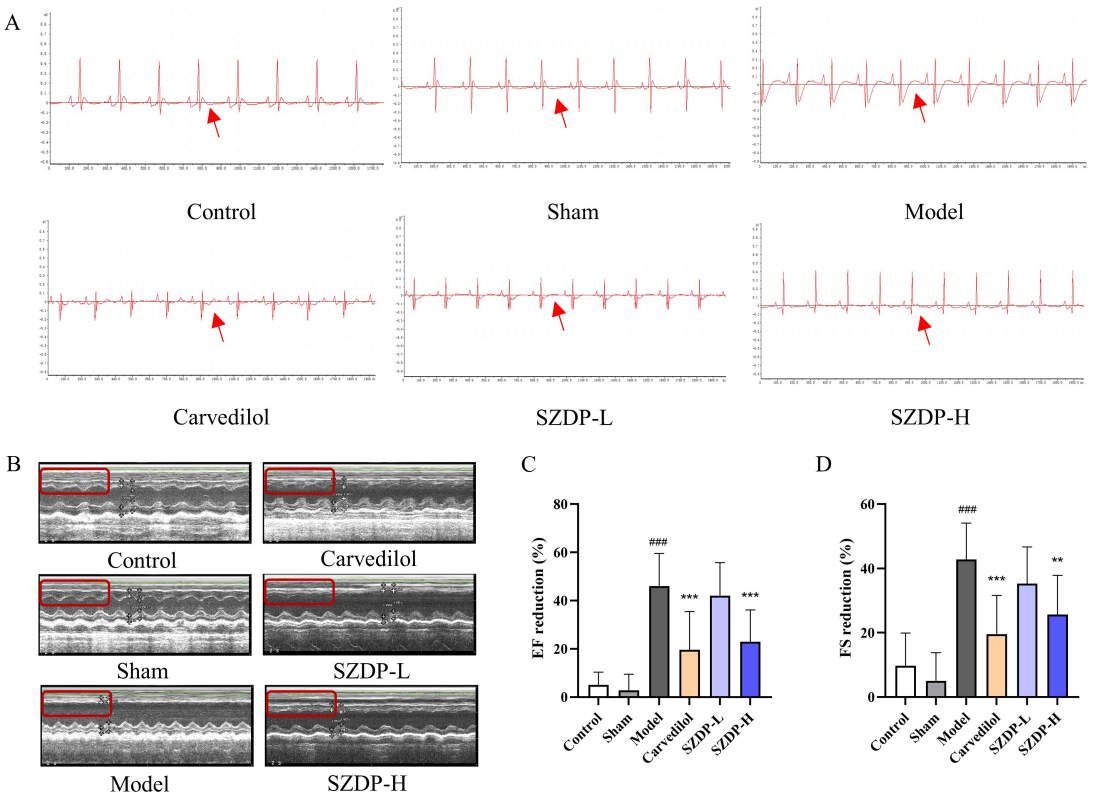

Figure 1 The ECG and echocardiography detection of rats. (A) Representative ECGs of rats in six groups. (B) Representative M-mode ultrasonic image in short-axis view of echocardiographic assay. (C) Reduction of EF (%). (D) Reduction of FS (%). Data are shown as Mean ± SD, (n = 9–11). $^{###}P < 0.001$ vs Sham group, $^{**}P < 0.01$, $^{***}P < 0.001$ vs Model group. SZDP, Shenzao dripping pill; EF, ejection fraction; FS, fractional shortening.

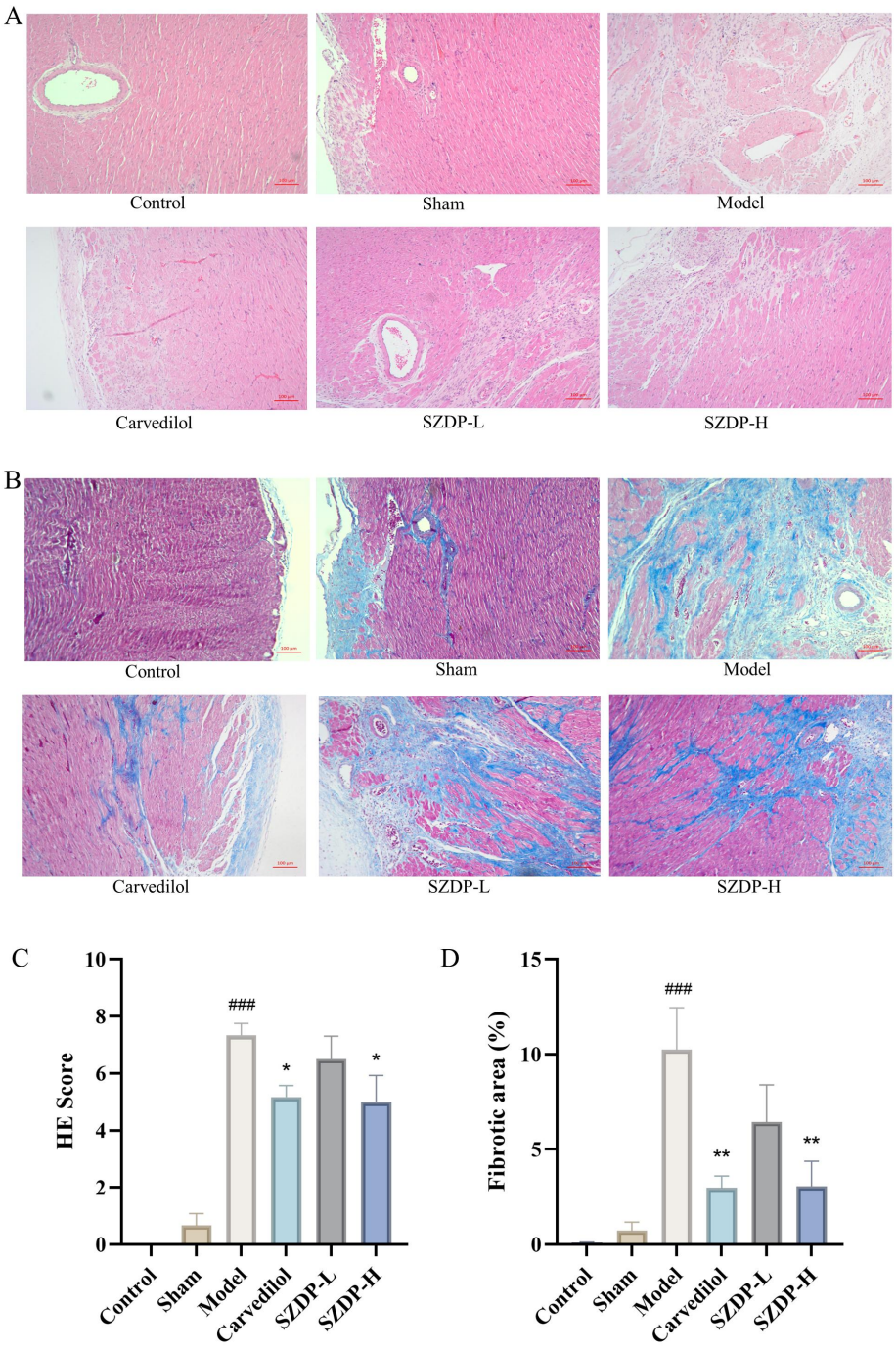

Figure 2 Representative results of pathologic changes in heart tissues. (A) H&E staining (Scales bar = 100 μm, magnification ×100). (B) Masson staining (Scales bar = 100 μm, magnification ×100). (C) Scores measurement of cardiomyocyte injury (n = 6). (D) Quantification of myocardial fibrotic area by Masson staining (n = 6). $^{###}P < 0.001$ vs Sham group, $^{*}P < 0.05$, $^{**}P < 0.01$ vs Model group. SZDP, Shenzao dripping pill; HE, hematoxylin and eosin staining.

The results demonstrated that the CMI model had been successfully established and that the symptoms of CMI in rats were significantly diminished following SZDP administration.

CMI can result in necrosis of the myocardium and the breaking of myocardial fibers, which are then replaced by collagen fibers in the interstitial spaces, leading to myocardial fibrosis. Masson staining is commonly used to differentiate collagen fibers from myocardial fibers. The findings of the study indicated that the control group did not exhibit any damage to the cardiac tissue, with well-arranged myocardial fibers and an absence of collagen fibers. The Sham group displayed partial fibrosis, but only a small amount of collagen was present in the deeper layers, likely due to partial damage to the myocardial surface during the chest opening procedure and inflammation caused by bleeding damage from threading, resulting in fibrosis in a limited area of the myocardium. The outer portion of the myocardial wall in the model group showed extensive myofibrosis, myocardial cell arrangement disorder, severe myocardial fiber lysis, and the presence of a few scattered erythrocytes in the intercellular space (Figure 2B). The Carvedilol group demonstrated a remarkable improvement in the distribution of collagen fibers compared to the model group. The SZDP-H group exhibited similar degrees of progress to the Carvedilol group, proving its effect in inhibiting myocardial fibrosis. The SZDP-L group showed more severe myocardial fibrosis than the SZDP-H group but less fiber lysis than the model group

Traditional Medicine Research 2024;9(11):62. https://doi.org/10.53388/TMR20240229002

(Figure 2D). Overall, all dosage groups of SZDP exhibited varying degrees of improvement in myocardial fibrosis.

Methods validation of untargeted metabolomics analysis

The QC samples were analyzed to confirm the method's reproducibility and the reliability of the data. The result of the base peak intensity chromatogram showed that the response intensity and retention time of chromatographic peaks from QC samples exhibited a significant overlap (Supplementary Figure S3A). The PCA plot illustrated a close clustering of QC samples in both positive and negative modes. These findings confirmed the excellent repeatability and stability of the instrument analysis throughout the experiment (Supplementary Figure S3B, S3C).

Multivariate statistical analysis of metabolomics data

PCA was utilized to find the overall difference between the datasets of the groups. The PCA score plot showed that all groups were not clearly separated from each other (Supplementary Figure S4A, S4B), but there was a partial trend, prompting the need for further analysis using OPLS-DA. OPLS-DA was employed to further distinguish metabolites and identify potential biomarkers from the comparison of the SZDP-H group, model group, and sham group. The OPLS-DA patterns across various serum samples showed significant separations between the Model and Sham groups in both positive and negative ion modes (Figure 3A, 3C), suggesting that CMI modelling disturbed rats' normal physiological metabolism and indicating that the establishing CMI model was successful at the metabolic level. The effectiveness of SZDP treatment in correcting the metabolic profiles in CMI rats was demonstrated by a clear separating trend between the SZDP-H and Model groups (Figure 3E, 3G), suggesting that administering the medium dose of SZDP changed the biochemical metabolism of CMI rats. The R2 and Q2 parameters were used to validate the OPLS-DA model's performance and accuracy. The results of the permutation tests (200 permutations) suggested that the OPLS-DA models were not overfitting and had reliable applicability (Figure 3B, 3D, 3F, 3H).

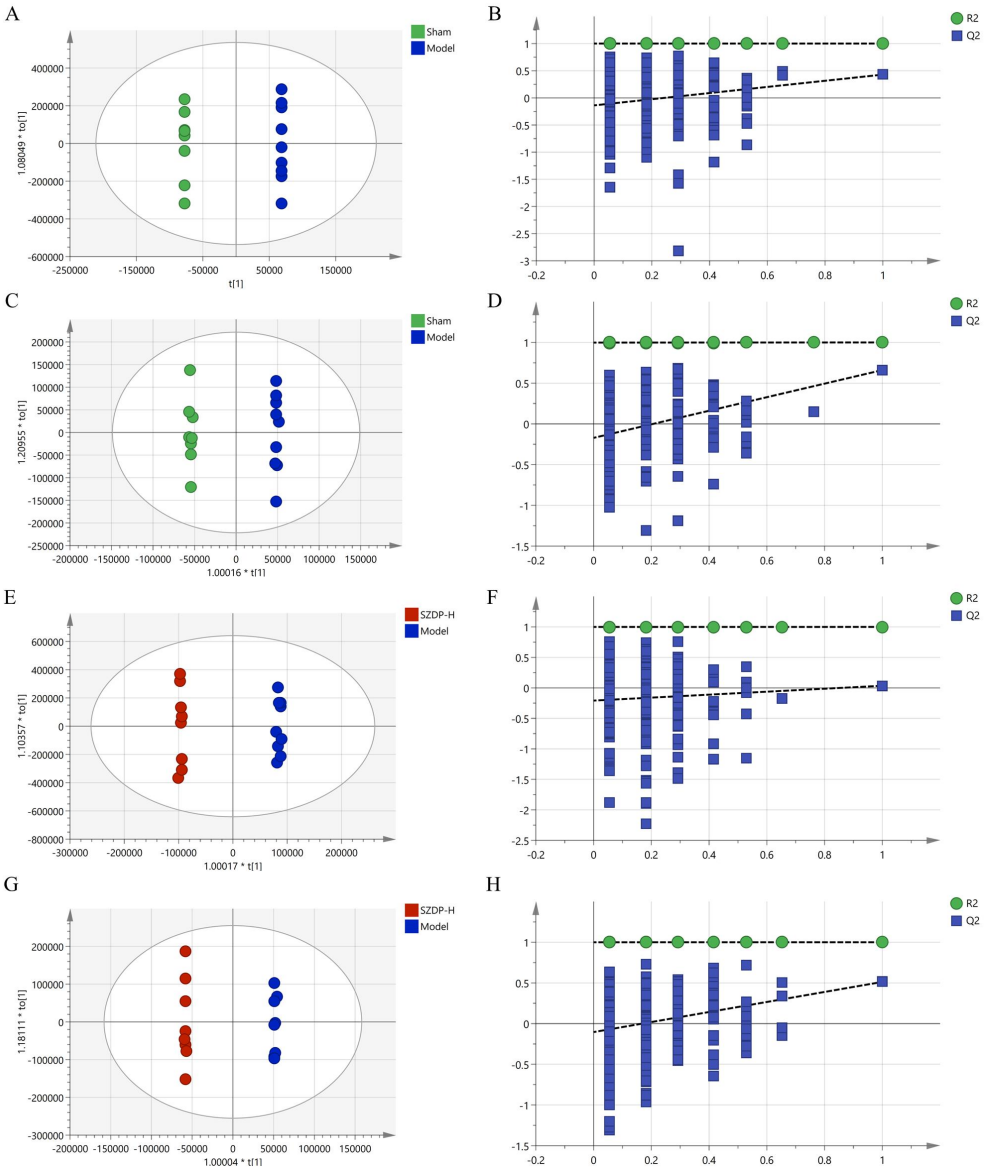

Figure 3 The Score plot of OPLS-DA and permutation test results. (A) OPLS-DA scores plot of Sham and Model groups in positive mode. (B) permutation test of positive mode of Sham and Model groups in positive mode (R2X = 0.99, R2Y = 1, Q2 = 0.428). (C) OPLS-DA scores plot of Sham and Model groups in negative mode. (D) permutation test of Sham and Model groups in negative mode (R2X = 0.514, R2Y = 0.999, Q2 = 0.66). (E) OPLS-DA scores plot of SZDP-H and Model groups in positive mode. (F) permutation test of SZDP-H and Model groups in positive mode (R2X = 0.81, R2Y = 0.999, Q2 = 0.0347). (G) OPLS-DA scores plot of SZDP-H and Model groups in negative mode. (H) permutation test of SZDP-H and Model groups in negative mode (R2X = 0.59, R2Y = 1, Q2 = 0.512). SZDP, Shenzao dripping pill.

Traditional Medicine Research 2024;9(11):62. https://doi.org/10.53388/TMR20240229002

Identification of potential biomarkers and metabolic pathways enrichment analysis

The values of VIP > 1 and $P < 0.05$ are used to assess the potential biomarkers between groups in the OPLS-DA analysis of metabolomics. The online database at HMDB (https://www.hmdb.ca) was used to screen the potential biomarkers by matching accurate mass and MS/MS fragment information within a 10 ppm error value. According to the above identification conditions, 17 differential metabolites as the potential biomarkers between the Sham and Model groups were identified, and 38 differential metabolites between the SZDP-H and Model groups were identified. Detailed differential metabolite results were summarized in Table 1, 2. Heatmap visualization showed the change in relative peak area levels of 55 differential metabolites (Figure 4A). Further observation showed that 10 differential metabolites were up-regulated in CMI rats, while 7 differential metabolites were down-regulated compared with the Sham group. And 32 differential metabolites were up-regulated by SZDP, while 6 differential metabolites were down-regulated compared with the model group. 13-Docosenamide was the common significant differential metabolite in the sham, model, and SZDP-H groups. However, we found that 5 candidate biomarkers were restored after SZDP administration, suggesting that the 6 metabolites in the sham, model, and SZDP-H groups exhibited the "high-low-high" or "low-high-low" trends, including Quinaldic acid, Estrone glucuronide, Leucylproline, 2,4,12-Octadecatrienoic acid, 6-Keto-decanoylcarnitine (Supplementary Figure S5).

Table 1 Identification results and information of blood biomarkers in CMI rats

No.	RT (min)	m/z	VIP	Compound name	Formula	HMDB ID	Change trend Model/Sham
1	5.98	352.2246	1.21	Prostaglandin E2	$C_{20}H_{32}O_5$	HMDB0001220	↑*
2	3.86	173.0476	1.29	Quinaldic acid	$C_{10}H_7NO_2$	HMDB0000842	↓**
3	17.09	337.3339	15.01	13-Docosenamide	$C_{22}H_{43}NO$	HMDB0244507	↓*
4	14.77	333.3027	1.58	2,4,12-Octadecatrienoic acid	$C_{22}H_{39}NO$	HMDB0032033	↓*
5	11.01	507.3684	3.75	LysoPC(P-18:0/0:0)	$C_{26}H_{54}NO_6P$	HMDB0013122	↑*
6	10.30	570.3512	1.08	Ganodermic acid P2	$C_{34}H_{50}O_7$	HMDB0035292	↓*
7	10.29	569.3473	1.88	LysoPC(22:5(4Z,7Z,10Z,13Z,16Z)/0:0)	$C_{30}H_{52}NO_7P$	HMDB0010402	↓*
8	1.12	228.1472	1.04	Leucylproline	$C_{11}H_{20}N_2O_3$	HMDB0011175	↓*
9	6.23	370.2352	1.74	Thromboxane B2	$C_{20}H_{34}O_6$	HMDB0003252	↑*
10	5.99	370.2350	2.74	Prostaglandin G1	$C_{20}H_{34}O_6$	HMDB0013039	↑*
11	5.66	430.2019	2.56	Armillarilin	$C_{24}H_{30}O_7$	HMDB0031673	↑*
12	4.84	188.0133	9.78	p-Cresol sulfate	$C_7H_8O_4S$	HMDB0011635	↑*
13	4.78	446.1969	1.23	Estrone glucuronide	$C_{24}H_{30}O_8$	HMDB0004483	↑*
14	4.77	329.4317	1.04	6-Keto-decanoylcarnitine	$C_{17}H_{31}NO_5$	HMDB0013202	↑*
15	19.67	326.1911	2.01	4-Dodecylbenzenesulfonic acid	$C_{18}H_{30}O_3S$	HMDB0059915	↓*
16	1.09	252.0841	1.63	Deoxyinosine	$C_{10}H_{12}N_4O_4$	HMDB0000071	↓*
17	0.89	650.5341	1.34	SM(d18:0/12:0)	$C_{35}H_{75}N_2O_6P$	HMDB0012084	↑**

Compared with Sham group, $^*P < 0.05$, $^{**}P < 0.01$. SZDP, Shenzao dripping pill; VIP, variable importance in projection.

Table 2 Identification results and information of blood biomarkers after SZDP administration

No.	RT (min)	m/z	VIP	Compound name	Formula	HMDB ID	Change trend SZDP/Model
1	6.19	348.1335	1.08	Diphenyl(2,4,6-trimethylbenzoyl) phosphine oxide	$C_{22}H_{21}O_2P$	HMDB0247372	↑*
2	6.19	312.1569	3.21	Propamidine	$C_{17}H_{20}N_4O_2$	HMDB0256810	↑**
3	6.19	358.1623	1.05	Xemilofiban	$C_{18}H_{22}N_4O_4$	HMDB0259927	↑**
4	6.13	454.2925	2.58	1-(4-O-beta-D-glucopyranosyl-3-methoxyphenyl)-3,5-dihydroxydecane	$C_{25}H_{42}O_7$	HMDB0303085	↑*
5	5.83	398.1546	1.55	Methyl (3x,10R)-dihydroxy-11-dodecene-6,8-diynoate 10-glucoside	$C_{19}H_{26}O_9$	HMDB0040896	↑**
6	5.83	388.1260	1.38	Aranidipine	$C_{19}H_{20}N_2O_7$	HMDB0248563	↑**
7	5.83	330.1675	7.04	tetranor-PGFM	$C_{16}H_{26}O_7$	HMDB0258925	↑**
8	5.82	366.1440	2.19	Tryptophan 2-C-mannoside	$C_{17}H_{22}N_2O_7$	HMDB0240296	↑**
9	5.82	393.1631	2.07	Erlotinib	$C_{22}H_{23}N_3O_4$	HMDB0014671	↑**
10	5.77	465.3084	1.24	Glycocholic acid	$C_{26}H_{43}NO_6$	HMDB0000138	↑*
11	5.62	214.0292	3.20	Deoxyribose 1-phosphate	$C_5H_{11}O_7P$	HMDB0001351	↑***
12	5.30	366.0405	1.62	Phosphoribosyl formamidocarboxamide	$C_{10}H_{15}N_4O_9P$	HMDB0001439	↑***
13	5.26	344.1465	3.45	Melibiitol	$C_{12}H_{24}O_{11}$	HMDB0006791	↑***
14	5.20	346.1625	2.40	Arginyl-glycyl-aspartic acid	$C_{12}H_{22}N_6O_6$	HMDB0248572	↑**
15	5.10	462.1159	1.29	Kaempferide 7-glucoside	$C_{22}H_{22}O_{11}$	HMDB0038455	↑***
16	5.06	326.1361	1.38	(2S,3S,4S,5R)-3,4,5-Trihydroxy-6-(5-methyl-2-propan-2-ylphenoxy) oxane-2-carboxylic acid	$C_{16}H_{22}O_7$	HMDB0255323	↑*
17	4.96	380.1234	1.58	3-O-Methylglycyrol	$C_{22}H_{20}O_6$	HMDB0033883	↑**
18	4.96	344.1467	6.12	Melibiitol	$C_{12}H_{24}O_{11}$	HMDB0006791	↑***
19	4.96	407.1424	1.85	N-Desmethyl Topotecan	$C_{22}H_{21}N_3O_5$	HMDB0255119	↑***
20	4.79	248.0715	1.28	2-(5'-methylthio) pentylmalate	$C_{10}H_{16}O_5S$	HMDB0304052	↑**
21	4.71	407.1425	1.10	N-Desmethyl topotecan	$C_{22}H_{21}N_3O_5$	HMDB0255119	↑**
22	4.37	371.1034	1.10	Triaminophenyl phosphate	$C_{18}H_{18}N_3O_4P$	HMDB0259149	↑*
23	6.29	406.2716	1.12	Alfaprostolum	$C_{24}H_{38}O_5$	HMDB0248132	↑*
24	4.54	150.0502	4.22	L-Xylulose	$C_5H_{10}O_5$	HMDB0000751	↑*
25	4.54	178.0450	3.78	L-Gulonolactone	$C_6H_{10}O_6$	HMDB0003466	↑*

Traditional Medicine Research 2024;9(11):62. https://doi.org/10.53388/TMR20240229002

Table 2 Identification results and information of blood biomarkers after SZDP administration (*continued*)

No.	RT (min)	m/z	VIP	Compound name	Formula	HMDB ID	Change trend SZDP/Model
26	4.35	371.1034	1.60	Aciclovir	$C_8H_{11}N_5O_3$	HMDB0014925	↑*
27	4.22	150.0502	1.99	D-Xylulose	$C_5H_{10}O_5$	HMDB0001644	↑*
28	3.14	204.0897	14.01	L-Tryptophan	$C_{11}H_{12}N_2O_2$	HMDB0000929	↑*
29	2.78	288.1019	1.84	Vanillyl mandelic acid	$C_{16}H_{16}O_5$	HMDB0259761	↑*
30	2.32	258.0915	2.00	2-(4-Hydroxy-3-phenoxyphenyl) propanoic acid	$C_{15}H_{14}O_4$	HMDB0246633	↑*
31	17.09	337.3339	8.24	13-Docosenamide	$C_{22}H_{43}NO$	HMDB0244507	↑*
32	13.12	537.3786	1.66	LysoPE(0:0/22:0)	$C_{27}H_{56}NO_7P$	HMDB0011490	↑*
33	12.47	316.2399	2.12	5beta-Pregnane-3,20-dione	$C_{21}H_{32}O_2$	HMDB0247019	↓**
34	11.50	330.2555	1.16	7,10,13,16,19-Docosapentaenoic acid	$C_{22}H_{34}O_2$	HMDB0247288	↓**
35	10.48	863.5636	1.35	PC (20:2(11Z,14Z)/PGJ2)	$C_{48}H_{82}NO_{10}P$	HMDB0287174	↓**
36	10.33	303.2276	1.83	Bornaprolol	$C_{19}H_{29}NO_2$	HMDB0249349	↓*
37	10.30	837.5480	2.86	PC (20:5(7Z,9Z,11E,13E,17Z)-3OH(5,6,15)/P-18:1(9Z))	$C_{46}H_{80}NO_{10}P$	HMDB0289808	↓**
38	0.82	103.1000	2.36	2-Amino-3-methyl-1-butanol	$C_5H_{13}NO$	HMDB0244984	↓**

Compared with Model group, $^{*}P < 0.05$, $^{**}P < 0.01$, $^{***}P < 0.001$. SZDP, Shenzao dripping pill; VIP, variable importance in projection.

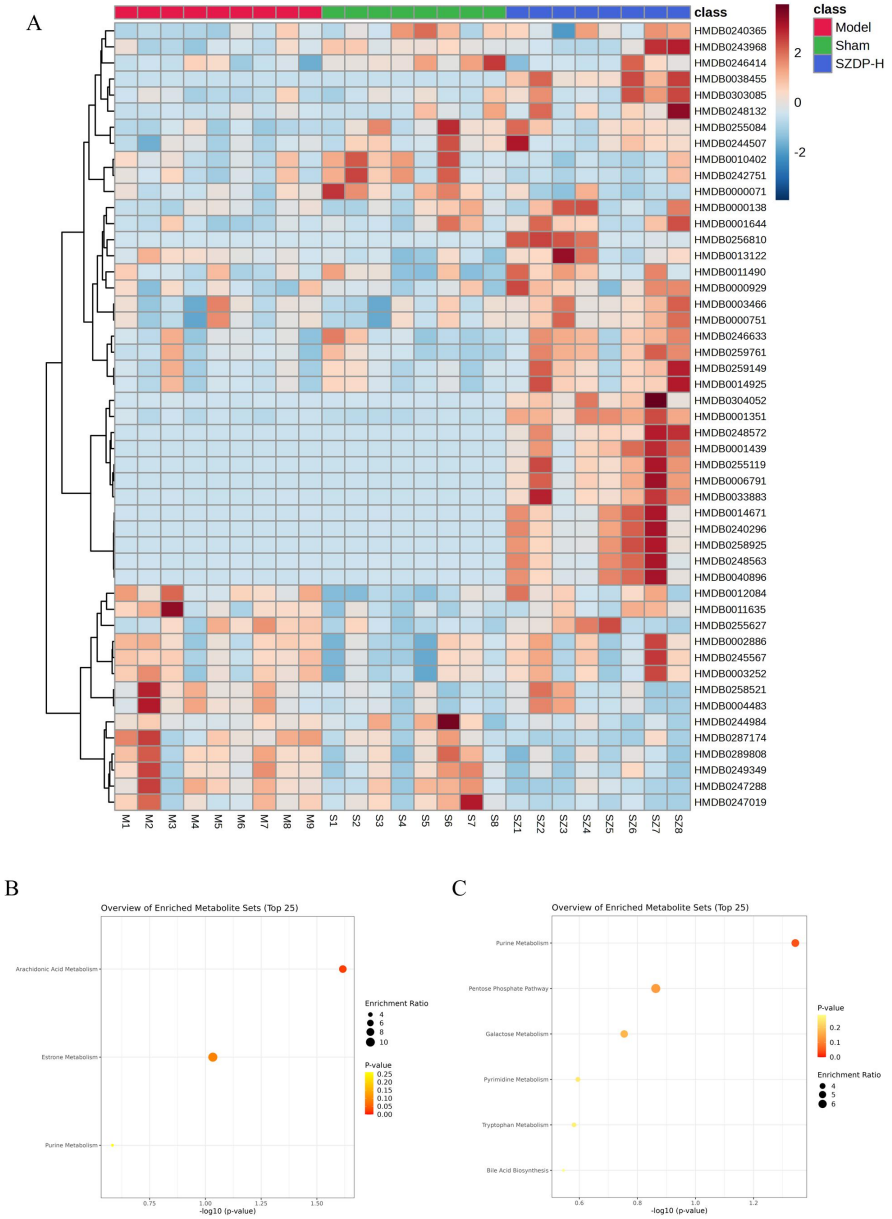

Figure 4 The pathway enrichment analysis and heatmap of identified differential metabolites. (A) Heatmap of identified differential metabolites. (B) Pathway enrichment analysis between the Sham and Model groups. (C) Pathway enrichment analysis between the SZDP-H and Model groups. SZDP, Shenzao dripping pill.

Traditional Medicine Research 2024;9(11):62. https://doi.org/10.53388/TMR20240229002

Metabolic pathway enrichment analysis was performed by MetaboAnalyst 4.0 for the differential metabolites. In the Sham and Model groups, there were three differential pathways (Figure 4B), including Arachidonic Acid Metabolism, Estrone Metabolism, and purine metabolism. Between the SZDP-H group and Model group, there were six differential pathways (Figure 4C), including Purine Metabolism, Pentose Phosphate Pathway, Galactose Metabolism, Pyrimidine Metabolism, Tryptophan Metabolism, and Bile Acid Biosynthesis. The metabolic pathway of Purine Metabolism was regulated in both CMI model and SZDP administration groups, suggesting that SZDP may affect this pathway for the treatment of CMI.

The network pharmacology study of SZDP against CMI

A total of 132 active components were obtained from six herbs of SZDP using the TCMSP database and SEA database. In addition, a total of 1,049 targets of the active components were obtained. A total of 7,170 CMI-related targets were obtained from the TDD, GeneCards, PharmGkb, DisGeNET, OCMIM, and DrugBank databases. Using the Venn online tool to match the CMI-related targets with the SZDP-related targets, 479 common targets were obtained (Supplementary Figure S6A). To create a PPI network map, the 479 targets were inputted into the String analysis tool (Supplementary Figure S6B). Then, the 479 targets were calculated with topological parameters of centrality for betweenness, closeness, degree, eigenvector, local average, and network. Then, a total of 31 key targets of SZDP treatment of CMI satisfied more than twice the median values of six parameters (Supplementary Figure S6C). To better demonstrate the connection between drugs and disease targets, we constructed an SZDP-herbs-compounds-targets-CMI network diagram (Figure 5A). In the GO enrichment analysis, a total of 157 items related to cell component (CC), 392 items related to molecular function (MF), and 3030 biological processes (BP) were identified. The results were performed by a ranking based on the *P* value, and the top 10 entries in BP, CC, and MF were shown (Figure 5B). The results showed that SZDP acted through various biological processes and molecular mechanisms, such as response to oxygen and nutrient levels, vascular process in the circulatory system, regulation of blood circulation, and oxidoreductase activity. According to the analysis of KEGG items, the top 30 pathways with the highest correlation were determined, signaling pathways such as Lipid and atherosclerosis and Fluid shear stress and atherosclerosis were mainly involved (Figure 5C). In this study, The KEGG analysis indicated that SZDP may improve the symptoms of CMI by mainly regulating lipid and atherosclerosis pathways to reduce lipid accumulation and promote blood circulation.

Integrated analysis of metabolomics and network pharmacology

A total of 48 common metabolic targets were screened from the sham versus model and SZDP versus model groups using enrichment analysis in MBRole 3.0. Combined with the 479 targets predicted by network pharmacology, TPMT, XDH, ATIC, and CYP1A1 were found to be four intersecting targets among the metabolic target, SZDP target, and CMI target categories (Figure 6A). To further reveal the relationship between metabolites, components, and targets, a "component-targets-metabolites" network was established (Figure 6B). There were 12 components and 3 differential metabolites associated with 4 key targets of TPMT, XDH, ATIC, and CYP1A1. The three key differential metabolites, Phosphoribosyl formamidocarboxamide, Deoxyribose 1-phosphate, and L-Tryptophan were up-regulated after SZDP administration (Supplementary Figure S7).

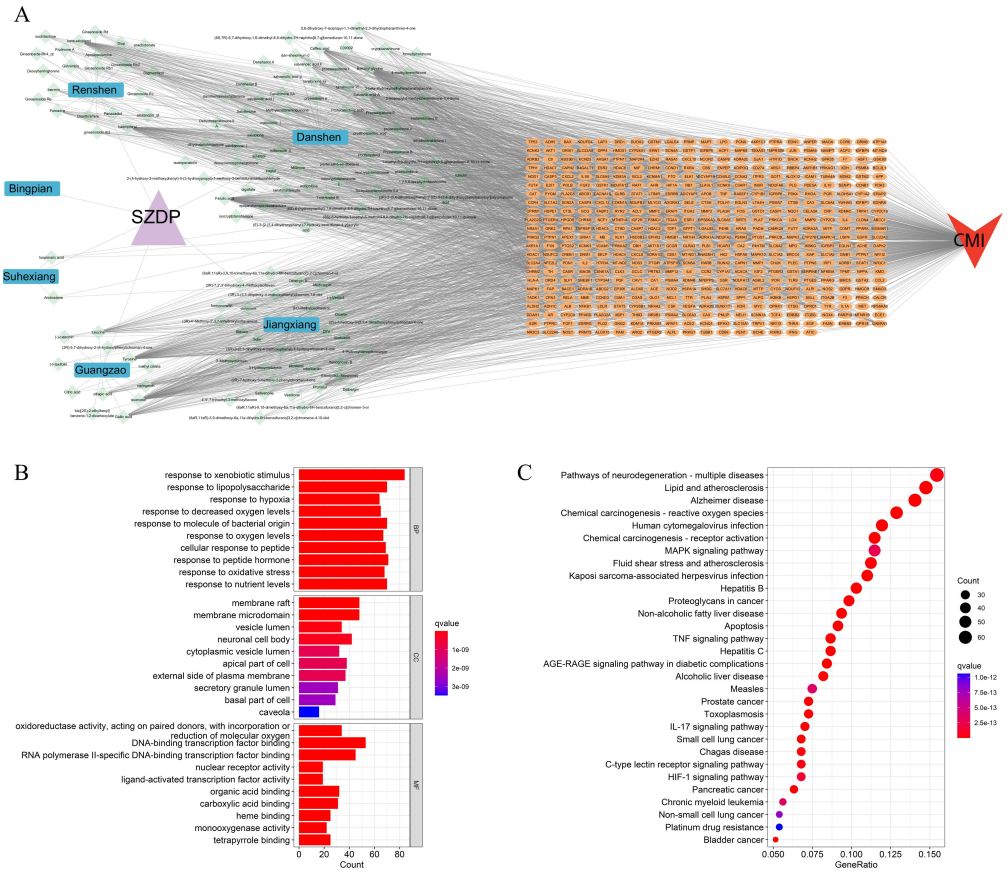

Figure 5 The network pharmacology study of SZDP against CMI. (A) SZDP-herbs-components-targets-MI network diagram, purple triangle node represented SZDP, blue rectangle nodes represented herbs, green diamond nodes represented compounds, orange circular nodes represented genes, and red V node represented MI. GO function (B) and KEGG pathway (C) enrichment analysis of SZDP-CMI targets. SZDP, Shenzao dripping pill; CMI, chronic myocardial ischemia; BP, biological process; CC, cell component; MF, molecular function.

Traditional Medicine Research 2024;9(11):62. https://doi.org/10.53388/TMR20240229002

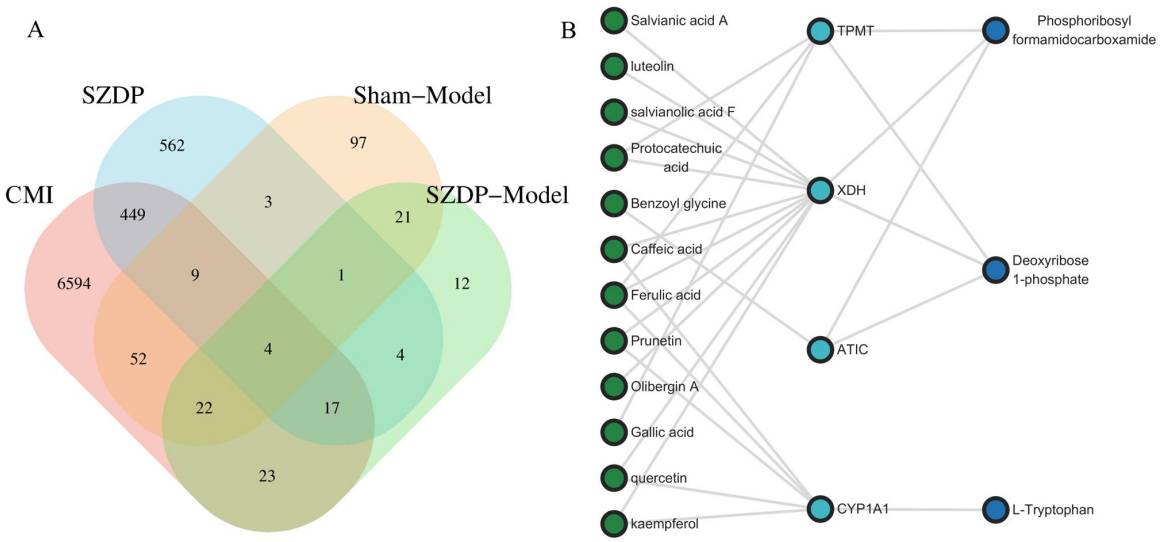

Figure 6 Discovery of potential targets between network pharmacology and metabolomic analysis. (A) Venny analysis of common targets from network pharmacology and serum metabolomic analysis. Blue elliptical involved SZDP targets, red elliptical involved CMI targets, orange elliptical involved Sham vs Model targets, green elliptical involved Sham vs Model targets. (B) Components-targets-metabolites relationship network. Dark green nodes represented components, light blue nodes represented genes, dark blue nodes represented differential metabolites. SZDP, Shenzao dripping pill; CMI, chronic myocardial ischemia; TPMT, thiopurine S-methyltransferase; XDH, xanthine dehydrogenase/oxidase; ATIC, bifunctional purine biosynthesis protein ATIC; CYP1A1, cytochrome p450 1A1.

Molecular docking confirmed that SZDP acted on key targets

According to the relationship network, TPMT, XDH, ATIC, and CYP1A1 were identified as the main targets of SZDP in the treatment of CMI. To further validate this, molecular docking was conducted on the four targets and their corresponding components to predict binding energy. In general, a binding energy less than −5.0 kcal/mol is considered a good affinity [30]. The results showed that all twelve components had strong binding ability to the relevant key targets (Figure 7A). Obviously, TPMT versus ferulic acid, XDH versus quercetin, ATIC versus benzoyl glycine, and CYP1A1 versus quercetin exhibited the strongest binding ability, thereby necessitating a visual analysis of these results (Figure 7B).

MD simulations revealed components-targets interactions

MD simulation was performed to further investigate the stability of the TPMT-ferulic acid, XDH-quercetin, ATIC-benzoyl glycine, and CYP1A1-quercetin complexes (Figure 8A). The root mean square deviation (RMSD) was performed to assess differences and changes in structure and evaluate the stability of the complexes (Figure 8B). The RMSD fluctuation range of the ATIC-benzoyl glycine complex was approximately 0.60 Å, the TPMT-ferulic acid complex was approximately 0.18 Å, and the XDH-quercetin and CYP1A1-quercetin complexes were approximately 0.25 Å. These results suggested that ferulic acid, quercetin, and benzoyl glycine exhibited strong stability upon binding to these key targets. Root mean square fluctuation (RMSF) was used to analyze the movement of amino acids. The RMSF values of the four complexes were relatively low, mostly kept at 0.1 to 0.6 Å (Figure 8C). The fluctuations of the TPMT-ferulic acid complex were relatively small compared with the others, so its relative stability was higher. The surface visualization conformations of the complexes in 100 ns during the period of MD simulation were displayed (Figure 8D), indicating that ferulic acid, quercetin, and benzoyl glycine remained at the center of the TPMT, XDH, ATIC, and CYP1A1 binding sites until the simulations were completed, suggesting there were stable interactions in the 4 complexes.

Discussion

CMI has become one of the most significant threats to human life because it reduces the function of the heart and induces myocardial infarction, myocardial fibrosis, and heart failure. Carvedilol belongs to the third class of β-receptor blockers, which can dilate blood vessels and inhibit apoptosis to protect the heart after ischemia [31]. Carvedilol was the positive control medicine that provided a reliable prerequisite for the experimental system. However, some adverse reactions will occur after Carvedilol administration [32]. The development of other anti-CMI drugs is valuable for patients who need to discontinue Carvedilol when adverse reactions occurred. TCM is preferred for the advantages of treatment by multi-target and multi-pathways. SZDP, as an empirical prescription to treat CMI, can regulate Qi, relieve pain, and promote blood circulation in the theory of TCM. The electrocardiography results demonstrated that the CMI model was successfully established and that the therapeutic effect of SZDP, as evidenced by ST-segment depression after modelling and ST elevation after SZDP administration, The left ventricle plays a dominant role in the pumping function of the heart, and the coronary ligation can lead to myocardial ischemia, even infarction in the left ventricle. The EF and FS indexes can reflect the left ventricle's pumping function. The echocardiography findings showed that SZDP administration significantly reduced the cardiac damage of CMI rats. The EF and FS indexes were reduced with significant differences in the model group, and the SZDP administration could significantly improve the reduction of EF and FS index as well as the positive medicine. Generally, AST, LDH, and CK are selected for acute myocardial injury measurements. However, no significant changes appeared in these biochemical indicators, possibly because of the compensatory response that would occur in a long-term model of myocardial infarction. After 28 days of myocardial ischemia, some cardiomyocytes died after ischemia and hypoxia, and fibroblasts secreted collagen fibers to replace the dead cardiomyocytes. Myocardial fibrosis was obvious, and the anterior wall of the myocardium was thinned, so it was not suitable to use TTC staining to analyze it. Myocardial infarction area calculated by TTC staining is the gold index for detection in acute myocardial infarction, but our study was a long-term myocardial infarction model, and the results of TTC staining could not reflect the results of the SZDP efficacy well, so the myocardial infarction area calculation was not carried out for this index. The HE and Masson staining results indicated that SZDP could decrease the degree of inflammatory cell infiltration, intercellular hemorrhage, cardiomyocyte injury, and myocardial fibrosis in CMI rats, showing similar results to those of positive control groups, which demonstrated SZDP may confer a cardioprotective effect to CMI.

Traditional Medicine Research 2024;9(11):62. https://doi.org/10.53388/TMR20240229002

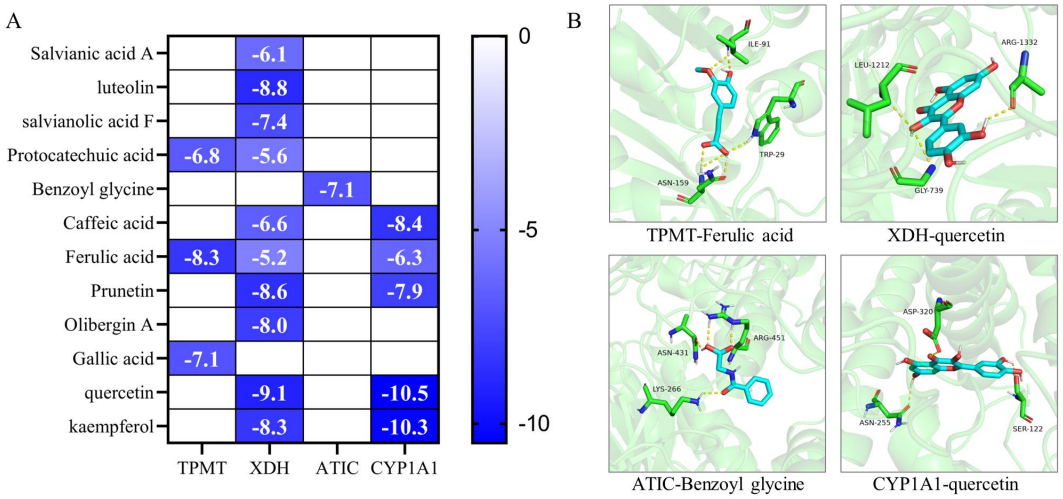

Figure 7 Molecular docking results. (A) The Binding Energy thermogram of associated components of SZDP with key targets. (B) Visualization of molecular docking. TPMT, thiopurine S-methyltransferase; XDH, xanthine dehydrogenase/oxidase; ATIC, bifunctional purine biosynthesis protein ATIC; CYP1A1, cytochrome p450 1A1.

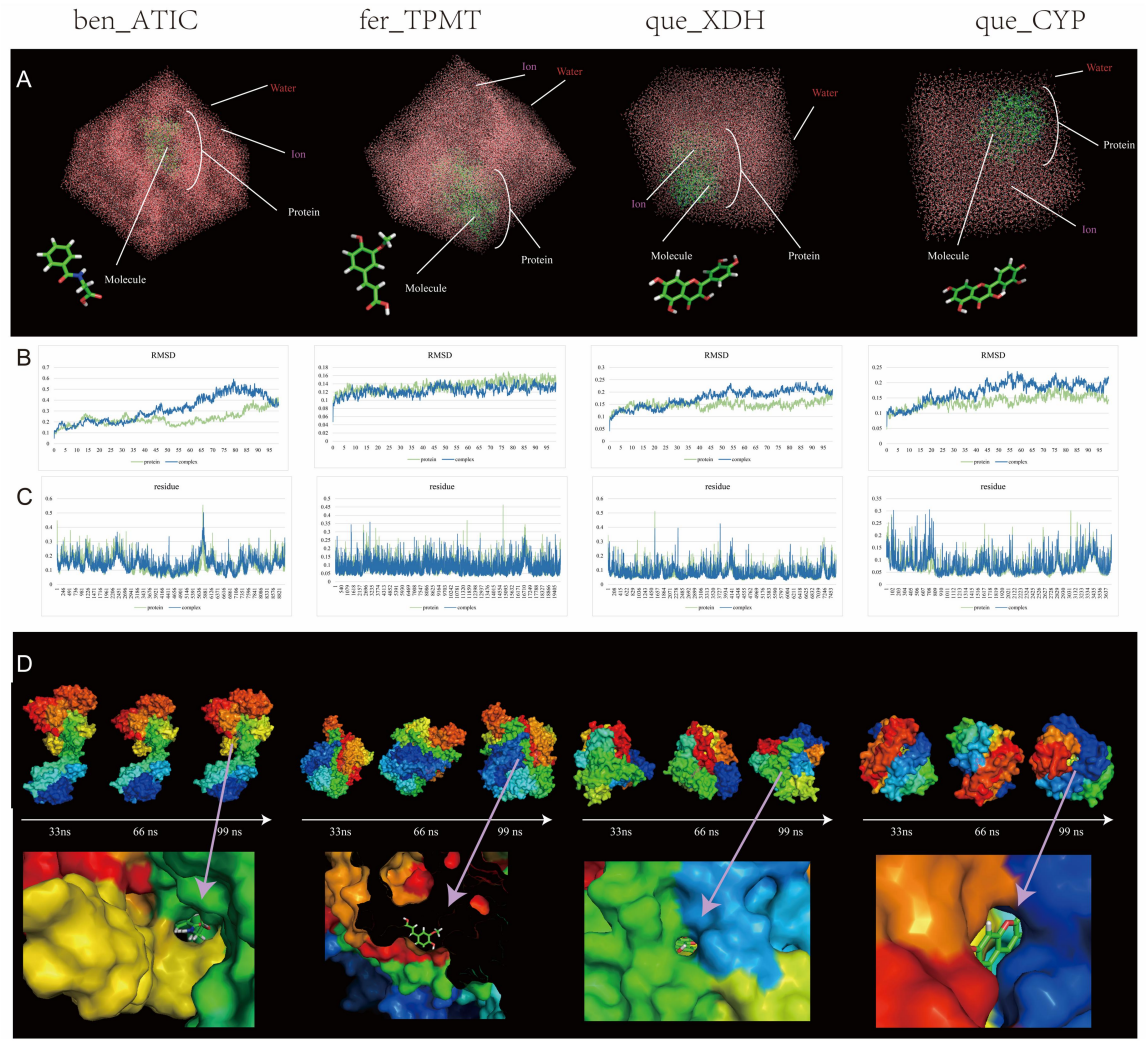

Figure 8 MD simulations results. (A) Visualization of MD simulations. Including the 3D structure of components, the box after charge-balancing ions containing water molecules, and the initial position of the components in the complex. (B) RMSD of all atoms of the key proteins (represented in green) in complex with the components of SZDP (represented in blue). (C) RMSF of all atoms of the key proteins (represented in green) in complex with the components of SZDP (represented in blue). (D) Surface visualization conformations of protein-component complexes at 0 and 100 ns. RMSD, root mean square deviation; TPMT, thiopurine S-methyltransferase; XDH, xanthine dehydrogenase/oxidase; ATIC, bifunctional purine biosynthesis protein ATIC; CYP1A1, cytochrome p450 1A1.

Metabolomics analysis revealed that SZDP effectively regulated six metabolites, and 13-Docosenamide was the common significant differential metabolite in the sham, model, and SZDP-H groups. 13-Docosenamide is a fatty acid amide and improves the imbalance of the hypothalamus-pituitary-adrenal axis [33]. The disorders of the hypothalamus-pituitary-adrenal axis lead to the increased changes in myocardial oxygen consumption and myocardial cell injury [34, 35]. Our results showed that the level of 13-Docosenamide was significantly decreased in model rats, and SZDP significantly reversed this change, suggesting that 13-Docosenamide may be the potential metabolic biomarker of the therapeutic application of SZDP for CMI. Network pharmacology was used to explore the possible mechanism of SZDP on CMI. In GO and KEGG analyses, SZDP regulated various biological processes and molecular mechanisms. Lipid and atherosclerosis and Fluid shear stress and atherosclerosis were identified as the important pathways, suggesting that SZDP may regulate these pathways to reduce lipid accumulation and promote blood circulation to treat CMI. Molecular docking results showed that the 12 key components can bind well with 4 key targets, suggesting that these key components were the effective ingredients of SZDP on treating CMI. The MD simulation results verified that there were robust interactions between the key targets and components. The mechanism underlying the treatment of CMI could be attributed to the binding of these active components to key targets, which therefore affects their activities and influences the production of downstream metabolic products.

Quercetin is a flavonoid that has anti-inflammatory, anti-coagulative, and anti-proliferative properties. Quercetin has been demonstrated that it can limit infarct size and prevent intramyocardial hemorrhage in clinical studies [36]. Additionally, it has been revealed that quercetin has prominent effects on ameliorating heart damage under myocardial ischemia conditions through different pathways [37, 38]. In our study, we found that quercetin had strong binding abilities to XDH and CYP1A1. Quercetin can regulate the activity of XDH to restore oxidative stress injury and reverse myocardial remodeling after myocardial ischemia [39]. Besides, quercetin can induce CYP1A1 expression [40]. Benzoyl glycine is significantly associated with left ventricular hypertrophy (LVH), and several pathophysiological mechanisms in LVH can lead to myocardial ischemia [41–43]. However, a causal relationship between benzoyl glycine and LVH is still unknown, and further work is required to confirm these findings. Ferulic acid is a polyphenolic compound that has cardioprotective effects [44]. Ferulic acid can modulate purine metabolism, improve oxidative stress, promote glutathione (GSH) production, and ameliorate myocardial infarction [45, 46].

Purine metabolism acted as the common metabolic pathway of SZDP in treating CMI in metabolomics. Purine metabolites can promote cell survival and proliferation by providing cells with the necessary energy and cofactors [47]. Purine nucleotides and their metabolites in vivo will increase significantly with the increment in myocardial energy consumption [48]. In purine metabolism, deoxyinosine is catalyzed to produce hypoxanthine and deoxyribose 1-phosphate. In our experiments, we found that the level of deoxyinosine decreased after CMI modeling, and the level of deoxyribose 1-phosphate increased significantly after SZDP administration. The results suggested that the consumption of deoxyinosine increased in the state of CMI, and the conversion of deoxyinosine to hypoxanthine and deoxyribose 1-phosphate could be promoted after the administration of SZDP. Quercetin can regulate the expression of XDH, which is able to catalyze the oxidation of hypoxanthine to xanthine and then further catalyze the oxidation of xanthine to uric acid [39, 49]. Uric acid has protective effects on CMI [50]. A study has demonstrated that the metabolites of the purine metabolism pathway, including xanthine, hypoxanthine, and uric acid, can inhibit the activity of acetylcholinesterase (AChE) [51]. AChE inhibition has cardioprotective actions that can reduce the risk of CMI and death from cardiovascular diseases [52, 53]. Additionally, the elevation of the 13-Docosenamide level had a positive correlation with AChE inhibition [54]. Thus, acting on XDH may be one of the mechanisms by which SZDP exerts its anti-CMI effects. Phosphoribosyl formamidocarboxamide (FAICAR) is one of the metabolites in purine metabolism. ATIC is a bifunctional enzyme that catalyzes the last two steps of purine biosynthesis [55]. The reaction between FAICAR and 5-aminoimidazole-4-carboxamide ribonucleotide (AICAR) is regulated by ATIC [56]. AICAR has been used to treat and protect against cardiac ischemic injury [57, 58]. In our study, we noted that the level of FAICAR in rats increased significantly after SZDP administration, suggesting that SZDP can likely play a role in the treatment of CMI by indirectly affecting the level of AICAR through its action on ATIC.

The enhancement of the level of Tryptophan is correlated with the activation of CYP1A1 [59, 60]. Higher levels of Tryptophan were inversely associated with mortality and fatal cardiovascular disease [61]. Our study notes that the L-Tryptophan levels in serum were markedly increased after SZDP administration, suggesting that SZDP may treat CMI by enhancing the levels of L-Tryptophan via the action of CYP1A1. CYP1A1 participates in the metabolism of fatty acids [62]. Meanwhile, TPMT alters S-adenosylmethionine consumption and consequently GSH synthesis that preserves fatty acid metabolism [63, 64]. Fatty acid oxidation is critical in myocardial energy generation, contributing to 40–80% of the heart's energy source [65]. To compensate for the lack of energy supply to the heart, fatty acid concentrations may significantly increase in ischemia and hypoxia conditions [66]. In our experiment, the levels of downstream metabolites of fatty acids, including 7,10,13,16,19-Docosapentaenoic acid, PC (20:2(11Z,14Z)/PGJ2), and PC (20:5(7Z,9Z,11E,13E,17Z)-3OH(5,6,15)/P-18:1(9Z)), were notably decreased after SZDP treatment. This indicated that SZDP can likely improve fatty acid metabolic abnormalities to treat CMI by targeting CYP1A1 and TPMT. Glucose metabolism disorder is one of the abnormal metabolisms when suffering from CMI. The Pentose phosphate pathway is one of the essential components of glucose metabolism. Some researchers have discovered that glucose becomes the primary energy source for myocardial energy metabolism during ischemic heart diseases [67, 68]. In this study, SZDP can regulate the production of deoxyribose 1-phosphate from the pentose phosphate pathway to improve the productive efficiency of glucose metabolism and relieve the insufficiency of myocardial energy, indicating that this may also be one of the mechanisms by which SZDP treats CMI.

In this study, we utilized pharmacodynamics, network pharmacology, and metabolomics to explore the anti-CMI effect of SZDP. We also used molecular docking technology to confirm the strong affinity of SZDP's pharmacodynamic components with the four key targets. However, the expression of related proteins remains unclear. In-depth molecular biology research on the mechanism of genes and proteins regulated by SZDP will be considered in the future to establish a further scientific basis for the anti-myocardial ischemic effect of SZDP.

Conclusions

This study explored the mechanism of SZDP in treating CMI using network pharmacology and metabolomics. SZDP could notably treat CMI caused by a blockage of coronary arteries and showed a similar protective effect as positive administration. 13-Docosenamide may be the potential metabolic biomarker of the therapeutic application of SZDP for CMI. The beneficial effects of SZDP in treating CMI were associated with up-regulating metabolite levels of Phosphoribosyl formamidocarboxamide, Deoxyribose 1-phosphate, and L-Tryptophan. TPMT, XDH, ATIC, and CYP1A1 may be the potential modulated targets in the treatment of CMI by SZDP. This study provides knowledge and a theoretical basis for further research on the mechanism of SZDP against CMI, supporting a reference for the application of SZDP in treating CMI.

References

1. Tsao CW, Aday AW, Almarzooq ZI, et al. Heart disease and stroke statistics – 2022 update: a report from the American

Heart Association. *Circulation.* 2022;145(8):e153–e639. Available at: http://doi.org/10.1161/CIR.0000000000001052
2. Vahdatpour C, Collins D, Goldberg S. Cardiogenic shock. *J Am Heart Assoc*. 2019;8(8):e011991. Available at: http://doi.org/10.1161/JAHA.119.011991
3. Marzilli M, Crea F, Morrone D, et al. Myocardial ischemia: From disease to syndrome. *Int J Cardiol.* 2020;314:32–35. Available at: http://doi.org/10.1016/j.ijcard.2020.04.074
4. Zhang F, Duan B, Zhou Z, et al. Integration of metabolomics and transcriptomics to reveal anti-chronic myocardial ischemia mechanism of Gualou Xiebai decoction. *J Ethnopharmacol.* 2022;297:115530. Available at: http://doi.org/10.1016/j.jep.2022.115530
5. Patel KN, Majmundar M, Vasudeva R, et al. Impact of Gender, Race, and Insurance Status on Inhospital Management and Outcomes in Patients With COVID-19 and ST-Elevation Myocardial Infarction (a Nationwide Analysis). *Am J Cardiol.* 2023;198:14–25. Available at: http://doi.org/10.1016/j.amjcard.2023.04.030
6. Feng WZ, Duan CC, Pan FZ, et al. Integration of metabolomics and network pharmacology to reveal the protective mechanism underlying Wogonoside in acute myocardial ischemia rats. *J Ethnopharmacol.* 2023;317:116871. Available at: http://doi.org/10.1016/j.jep.2023.116871
7. Li X, Yu T, Jiang Q, Tan J, Liu K. The Efficacy of Traditional Chinese Herbal Medicine Across Multiple Cardiovascular Diseases: An Umbrella Review of Systematic Reviews of Randomized Controlled Trials. *J Cardiovasc Pharmacol.* 2024;83(4):340–52. Available at: http://doi.org/10.1097/FJC.0000000000001535
8. Huang X, Zhang M, Song Y, et al. Integrated network pharmacology to investigate the mechanism of Salvia miltiorrhiza Bunge in the treatment of myocardial infarction. *J Cell Mol Med.* 2023;27(22):3514–3525. Available at: http://doi.org/10.1111/jcmm.17932
9. Jia QJ, Wang LR, Zhang XN, et al. Prevention and treatment of chronic heart failure through traditional Chinese medicine: Role of the gut microbiota. *Pharmacol Res.* 2020;151:104552. Available at: http://doi.org/10.1016/j.phrs.2019.104552
10. Tan YQ, Chen HW, Li J. Astragaloside IV: an effective drug for the treatment of cardiovascular diseases. *Drug Des Devel Ther.* 2020;14:3731–3746. Available at: http://doi.org/10.2147/DDDT.S272355
11. Wang YM, Li X, Qi M, et al. Pharmacological effects and mechanisms of YiYiFuZi powder in chronic heart disease revealed by metabolomics and network pharmacology. *Front Mol Biosci.* 2023;10:1203208. Available at: http://doi.org/10.3389/fmolb.2023.1203208
12. Hu T, Liu Q, Zeng X, et al. Study on the quality standard of Shenzao dripping pills. *J Guangdong Pharm Univ.* 2022;38(1):51–56. Available at: http://doi.org/10.16809/j.cnki.2096-3653.2021120204
13. Xu H, Yu SL, Lin CX, et al. Roles of flavonoids in ischemic heart disease: Cardioprotective effects and mechanisms against myocardial ischemia and reperfusion injury. *Phytomedicine.* 2024;126:155409. Available at: http://doi.org/10.1016/j.phymed.2024.155409
14. Sun B, Xia QM, Gao ZY. Total flavones of Choerospondias axillaris attenuate cardiac dysfunction and myocardial interstitial fibrosis by modulating NF-κB signaling pathway. *Cardiovasc Toxicol.* 2015;15(3):283–289. Available at: http://doi.org/10.1007/s12012-014-9298-3
15. Chen J, Wang YC, Wang SF, Zhao XP, Zhao L, Wang Y. Salvianolic acid B and ferulic acid synergistically promote angiogenesis in HUVECs and zebrafish via regulating VEGF signaling. *J Ethnopharmacol.* 2022;283:114667. Available at: http://doi.org/10.1016/j.jep.2021.114667
16. Zheng XJ, Liu HM, Ma MQ, Ji JB, Zhu FL, Sun LR. Anti-thrombotic activity of phenolic acids obtained from Salvia miltiorrhiza f. alba in TNF-α-stimulated endothelial cells via the NF-κB/JNK/p38 MAPK signaling pathway. *Arch Pharm Res.* 2021;44(4):427–438. Available at: http://doi.org/10.1007/s12272-021-01325-7
17. Lei W, Li X, Li L, et al. Compound Danshen Dripping Pill ameliorates post ischemic myocardial inflammation through synergistically regulating MAPK, PI3K/AKT and PPAR signaling pathways. *J Ethnopharmacol.* 2021;281:114438. Available at: http://doi.org/10.1016/j.jep.2021.114438
18. Li M, Li XW, Zhou LM, Jin YR. Effects of total saponins from Panacis majoris Rhizoma and its degradation products on myocardial ischemia-reperfusion injury in rats. *Biomed Pharmacother.* 2020;130:110538. Available at: http://doi.org/10.1016/j.biopha.2020.110538
19. Zhou Z, Shen WX, Yu LL, Xu C, Wu QB. A Chinese patent medicine, Shexiang Baoxin Pill, for Non-ST-elevation acute coronary syndromes: A systematic review. *J Ethnopharmacol.* 2016;194:1130–1139. Available at: http://doi.org/10.1016/j.jep.2016.11.024
20. Lin R, Duan JL, Mu F, et al. Cardioprotective effects and underlying mechanism of Radix Salvia miltiorrhiza and Lignum Dalbergia odorifera in a pig chronic myocardial ischemia model. *Int J Mol Med.* 2018;42(5):2628–2640. Available at: http://doi.org/10.3892/ijmm.2018.3844
21. Yu YH, Sun JH, Liu JG, Wang PL, Wang CL. Ginsenoside Re preserves cardiac function and ameliorates left ventricular remodeling in a rat model of myocardial infarction. *J Cardiovasc Pharmacol.* 2020;75(1):91–97. Available at: http://doi.org/10.1097/FJC.0000000000000752
22. Hu T, Zheng KN, Liang JY, et al. Integrated UHPLC-MS and network pharmacology to explore the active constituents and pharmacological mechanisms of Shenzao dripping pills against coronary heart disease. *Tradit Med Res.* 2022;7(3):24. Available at: http://doi.org/10.53388/TMR20220308267
23. Xian MH, Zheng KN, Zhan SK, Liang JY, Wang SF. Analysis of volatile components in compound Shenzao dripping pills by GC-MS. *Guangdong Chem Ind.* 2021;48(16):249–252. (Chinese) Available at: https://kns.cnki.net/kcms2/article/abstract?v=Xhw-7KfLOFlm_drgv2866nMeU95QlNe6UbWM8bt9wbfRgtVxO8vDKe618fUdaixz1ttsIxvAjFPXreNv8NQeZI3dFIwF6EXr4CLqgFIQHfgGflxRQORfr3eDpo5yPIfPF0L-WedZECrtqnwuQPyk3w==&uniplatform=NZKPT&language=CHS
24. Marzilli M. Myocardial energy balance and metabolism as causes of myocardial ischemia. *Vascul Pharmacol.* 2024;154:107273. Available at: http://doi.org/10.1016/j.vph.2023.107273
25. Hasselbalch RB, Kristensen JH, Strandkjær N, et al. Metabolomics of early myocardial ischemia. *Metabolomics.* 2023;19(4):33. Available at: http://doi.org/10.1007/s11306-023-01999-8
26. Huang SM, Li ZX, Jiang SR, Xu MW. Metabolomic study on the protective effect of isoorientin against myocardial infarction. *Biochem Biophys Res Commun.* 2022;598:81–88. Available at: http://doi.org/10.1016/j.bbrc.2022.02.008
27. Gao JY, Wang YY, Xiong H, et al. Uncovering the mechanism of Chinese Hawthorn leaf on myocardial ischemia based on network pharmacology, molecular docking verification, and in vitro studies. *Cardiovasc Toxicol.* 2024;24(2):171–183. Available at: http://doi.org/10.1007/s12012-024-09825-w
28. Deng L, Duan YX, Liu C, Sun JJ, Zhao SH, Deng J. Mechanism of Artemisia annua L. in the treatment of acute myocardial infarction: network pharmacology, molecular docking and in vivo validation. *Mol Divers.* 2023. Available at:

http://doi.org/10.1007/s11030-023-10750-3
29. Wang WL, Chen Y. Network pharmacology prediction and molecular docking-based strategy to explore the potential mechanism of Gualou Xiebai Banxia decoction against myocardial infarction. *Genes.* 2024;15(4):392. Available at: http://doi.org/10.3390/genes15040392
30. Yang MX, Sun SL, Jia XM, et al. Study on mechanism of hepatoprotective effect of Chrysanthemum morifolium Ramat. based on metabolomics with network analysis and network pharmacology. *J Chromatogr B Analyt Technol Biomed Life Sci.* 2023;1222:123711. Available at: http://doi.org/10.1016/j.jchromb.2023.123711
31. Bayoumi AS, Park K, Wang Y, et al. A carvedilol-responsive microRNA, miR-125b-5p protects the heart from acute myocardial infarction by repressing pro-apoptotic bak1 and klf13 in cardiomyocytes. *J Mol Cell Cardiol.* 2018;114:72–82. Available at: http://doi.org/10.1016/j.yjmcc.2017.11.003
32. Maharaj S, Seegobin K, Perez-Downes J, Bajric B, Chang S, Reddy P. Severe carvedilol toxicity without overdose – caution in cirrhosis. *Clin Hypertens.* 2017;23(1):25. Available at: http://doi.org/10.1186/s40885-017-0083-z
33. Li MM, Jiang Z, Song LY, Quan ZS, Yu HL. Antidepressant and anxiolytic-like behavioral effects of erucamide, a bioactive fatty acid amide, involving the hypothalamus–pituitary–adrenal axis in mice. *Neurosci Lett.* 2017;640:6–12. Available at: http://doi.org/10.1016/j.neulet.2016.12.072
34. Goico A, Chandrasekaran M, Herrera CJ. Novel developments in stress cardiomyopathy: From pathophysiology to prognosis. *Int J Cardiol.* 2016;223:1053–1058. Available at: http://doi.org/10.1016/j.ijcard.2016.08.241
35. Headrick JP, Peart JN, Budiono BP, Shum DHK, Neumann DL, Stapelberg NJC. The heartbreak of depression: 'Psycho-cardiac' coupling in myocardial infarction. *J Mol Cell Cardiol.* 2017;106:14–28. Available at: http://doi.org/10.1016/j.yjmcc.2017.03.007
36. Kozhukhov S, Parkhomenko A, Lutay Y, Dovganych N. Impact of quercetin in patients with myocardial infarction. A multicenter, randomized, and open-label pilot study. *Hellenic J Cardiol.* 2024;76:68–74. Available at: https://pubmed.ncbi.nlm.nih.gov/37567562/
37. Liu CY, Huang JG, Qiu JX, et al. Quercitrin improves cardiac remodeling following myocardial infarction by regulating macrophage polarization and metabolic reprogramming. *Phytomedicine.* 2024;127:155467. Available at: http://doi.org/10.1016/j.phymed.2024.155467
38. Farazi MM, Rostamzadeh F, Jafarinejad-Farsangi S, Moazam Jazi M, Jafari E, Gharbi S. CircPAN3/miR-221/PTEN axis and apoptosis in myocardial infarction: Quercetin's regulatory effects. *Gene.* 2024;909:148316. Available at: http://doi.org/10.1016/j.gene.2024.148316
39. Zhang YM, Zhang ZY, Wang RX. Protective mechanisms of quercetin against myocardial ischemia reperfusion injury. *Front Physiol.* 2020;11:956. Available at: http://doi.org/10.3389/fphys.2020.00956
40. Vrba J, Kren V, Vacek J, Papouskova B, Ulrichova J. Quercetin, quercetin glycosides and taxifolin differ in their ability to induce AhR activation and CYP1A1 expression in HepG2 cells. *Phytother Res.* 2012;26(11):1746–1752. Available at: http://doi.org/10.1002/ptr.4637
41. Yu TH, Tang WH, Lu YC, et al. Association between hippuric acid and left ventricular hypertrophy in maintenance hemodialysis patients. *Clin Chim Acta.* 2018;484:47–51. Available at: http://doi.org/10.1016/j.cca.2018.05.022
42. Mølgaard S, Faricelli B, Salomonsson M, Engstrøm T, Treiman M. Increased myocardial vulnerability to ischemia–reperfusion injury in the presence of left ventricular hypertrophy. *J Hypertens.* 2016;34(3):513–523. Available at: http://doi.org/10.1097/HJH.0000000000000826
43. Koracevic G, Mićić S, Stojanovic M, et al. Significance of beta-blocker in patients with hypertensive left ventricular hypertrophy and myocardial ischemia. *Curr Vasc Pharmcol.* 2023;21(2):81–90. Available at: http://doi.org/10.2174/1570161121666230201141215
44. Wang F, Peng Q, Liu J, Alolga RN, Zhou W. A novel ferulic acid derivative attenuates myocardial cell hypoxia reoxygenation injury through a succinate dehydrogenase dependent antioxidant mechanism. *Eur J Pharmacol.* 2019;856:172417. Available at: http://doi.org/10.1016/j.ejphar.2019.172417
45. Liu XL, Qi K, Gong Y, et al. Ferulic acid alleviates myocardial ischemia reperfusion injury via upregulating AMPKα2 expression-mediated ferroptosis depression. *J Cardiovasc Pharmacol.* 2021;79(4):489–500. Available at: http://doi.org/10.1097/FJC.0000000000001199
46. Salau VF, Erukainure OL, Ibeji CU, Olasehinde TA, Koorbanally NA, Islam MdS. Ferulic acid modulates dysfunctional metabolic pathways and purinergic activities, while stalling redox imbalance and cholinergic activities in oxidative brain injury. *Neurotox Res.* 2020;37(4):944–955. Available at: http://doi.org/10.1007/s12640-019-00099-7
47. Pedley AM, Benkovic SJ. A new view into the regulation of purine metabolism: the purinosome. *Trends Biochem Sci.* 2017;42(2):141–154. Available at: http://doi.org/10.1016/j.tibs.2016.09.009
48. Zhen JT, Fan YY, Zhao XL, et al. Effect of ciclosporin A on purine metabolism in rats with myocardial ischemia-reperfusion injury. *J Tianjin Med Univ.* 2012;18(1):37–39 + 43. (Chinese) Available at: http://doi.org/10.3969/j.issn.1006-8147.2012.01.012
49. Dissanayake LV, Spires DR, Levchenko V, Khedr S, Palygin O, Staruschenko A. The role of Xanthine Dehydrogenase (XDH) and uric acid in the kidney development and renal injury. *FASEB J.* 2020;34(S1):1. Available at: http://doi.org/10.1096/fasebj.2020.34.s1.02973
50. Ma PQ, Zhao MH, Li Y, et al. The protective effects of uric acid against myocardial ischemia via the Nrf2 pathway. *Eur J Pharmacol.* 2023;959:176062. Available at: http://doi.org/10.1016/j.ejphar.2023.176062
51. Mazumder MK, Phukan BC, Bhattacharjee A, Borah A. Disturbed purine nucleotide metabolism in chronic kidney disease is a risk factor for cognitive impairment. *Med Hypotheses.* 2018;111:36–39. Available at: http://doi.org/10.1016/j.mehy.2017.12.016
52. Rampa L, Santangelo R, Gaspardone C, et al. Potential cardiologic protective effects of acetylcholinesterase inhibitors in patients with mild to moderate dementia. *Am J Cardiol.* 2023;200:162–170. Available at: http://doi.org/10.1016/j.amjcard.2023.05.041
53. Rampa L, Gaspardone C, Fiore G, et al. Potential cardioprotective effects of acetylcholinesterase inhibitors in patients with Alzheimer's disease. *Eur Heart J.* 2023;44(S2):ehad655.2654. Available at: http://doi.org/10.1093/eurheartj/ehad655.2654
54. Kim CR, Kim HS, Choi SJ, et al. Erucamide from radish leaves has an inhibitory effect against acetylcholinesterase and prevents memory deficit induced by trimethyltin. *J Med Food.* 2018;21(8):769–776. Available at: http://doi.org/10.1089/jmf.2017.4117
55. Vergis JM, Beardsley GP. Catalytic mechanism of the cyclohydrolase activity of human aminoimidazole carboxamide ribonucleotide formyltransferase/inosine monophosphate cyclohydrolase. *Biochemistry.* 2004;43(5):1184–1192. Available at: http://doi.org/10.1021/bi035139b
56. Mazzarino RC, Baresova V, Zikánová M, et al. The CRISPR-Cas9 crATIC HeLa transcriptome: Characterization of a novel cellular

model of ATIC deficiency and ZMP accumulation. *Mol Genet Metab Rep.* 2020;25:100642. Available at: http://doi.org/10.1016/j.ymgmr.2020.100642
57. Wang ZF, Cao YK, Yin Q, et al. Activation of AMPK alleviates cardiopulmonary bypass-induced cardiac injury via ameliorating acute cardiac glucose metabolic disorder. *Cardiovasc Ther.* 2018;36(6):e12482. Available at: http://doi.org/10.1111/1755-5922.12482
58. Inata Y, Piraino G, Hake PW, et al. Age-dependent cardiac function during experimental sepsis: effect of pharmacological activation of AMP-activated protein kinase by AICAR. *Am J Physiol Heart Circ Physiol.* 2018;315(4):H826–H837. Available at: http://doi.org/10.1152/ajpheart.00052.2018
59. Haduch A, Bromek E, Kuban W, Daniel WA. The engagement of cytochrome P450 enzymes in tryptophan metabolism. *Metabolites.* 2023;13(5):629. Available at: http://doi.org/10.3390/metabo13050629
60. Liang H, Dai Z, Liu N, et al. Dietary L-tryptophan modulates the structural and functional composition of the intestinal microbiome in weaned piglets. *Front Microbiol.* 2018;9:1736. Available at: http://doi.org/10.3389/fmicb.2018.01736
61. Teunis CJ, Stroes ESG, Boekholdt SM, et al. Tryptophan metabolites and incident cardiovascular disease: The EPIC-Norfolk prospective population study. *Atherosclerosis.* 2023;387:117344. Available at: http://doi.org/10.1016/j.atherosclerosis.2023.117344
62. Lucas D, Goulitquer S, Marienhagen J, et al. Stereoselective epoxidation of the last double bond of polyunsaturated fatty acids by human cytochromes P450. *J Lipid Res.* 2010;51(5):1125–1133. Available at: http://doi.org/10.1194/jlr.M003061
63. Liu YF, Wu KM, Fu YK, Li WY, Zhao XY. Slc7a11 stimulates glutathione synthesis to preserve fatty acid metabolism in primary hepatocytes. *Redox Rep.* 2023;28(1):2260646. Available at: http://doi.org/10.1080/13510002.2023.2260646
64. Šmid A, Štajdohar M, Milek M, et al. Transcriptome analysis reveals involvement of thiopurine S-methyltransferase in oxidation-reduction processes. *Eur J Pharm Sci.* 2024;192:106616. Available at: http://doi.org/10.1016/j.ejps.2023.106616
65. Wang YF, Sun WT, Zheng JL, et al. Urinary metabonomic study of patients with acute coronary syndrome using UPLC-QTOF/MS. *J Chromatogr B Analyt Technol Biomed Life Sci.* 2018;1100–1101:122–130. Available at: http://doi.org/10.1016/j.jchromb.2018.10.005
66. Sun M, Liu W, Liu HX, Yu B. Study on plasma metabolomics of patients with early-stage coronary atherosclerosis. *Chin Circ J.* 2022;37(1):24–30. Available at: http://doi.org/10.3969/j.issn.1000-3614.2022.01.004
67. Li J, Zhong SJ, Li L, et al. Biological basic research on model rats of coronary heart disease with blood stasis syndrome based on urine metabolomics. *Chin J Inf Tradit Chin Med.* 2021;28(3):63–68. Available at: http://doi.org/10.19879/j.cnki.1005-5304.202008389
68. Guo ZJ, Wang M, Ying XD, et al. Caloric restriction increases the resistance of aged heart to myocardial ischemia/reperfusion injury via modulating AMPK–SIRT1–PGC1a energy metabolism pathway. *Sci Rep.* 2023;13(1):2045. Available at: http://doi.org/10.1038/s41598-023-27611-6